JASs Journal of Anthropological Sciences Open Access
Research articles Vol. 104 (2026), pp. 1 - 22 e-pub ahead of print doi. 10.4436/jass.10403

The anatomical position of the ribs and thoracic vertebrae of the Roc de Marsal Neandertal infant

Asier Gómez-Olivencia[1,2,3] & Daniel García-Martínez[4,5]

1) Dept. Geología, Facultad de Ciencia y Tecnología, Universidad del País Vasco/Euskal Herriko Unibertsitatea (UPV/EHU), Leioa, Spain
e-mail: asier.gomezo@ehu.eus

2) Centro Mixto UCM-ISCIII de Evolución y Comportamiento Humanos, Madrid 28029, Spain

3) Sociedad de Ciencias Aranzadi, Donostia-San Sebastián, Spain

4) Physical Anthropology Unit, Department of Biodiversity, Ecology, and Evolution, Faculty of Biological Sciences, Complutense University of Madrid, Madrid, Spain

5) Laboratory of Forensic Anthropology, Centre for Functional Ecology, Department of Life Sciences, University of Coimbra, Coimbra, Portugal

Summary - *Recent technical and methodological advances have provided new insights into Neandertal thorax morphology, revealing significant differences compared to modern humans, both in terms of the individual elements (vertebrae, ribs, and sternum), and in the thorax as a whole. However, the thorax morphology of immature Neandertals remains poorly understood, due to the limited and fragmentary fossil record. The Roc de Marsal (RdM) infant is one of the few cases in which the vertebrae and ribs are both relatively well preserved. Previous research has characterised the ribs of the RdM individual as having shafts with low robusticity and short necks. They also have a large radius of curvature (i.e., they are less curved) and a pronounced anterior flare. Theoretically, this would result in a thorax that was more antero-posteriorly projected than that of* Homo sapiens*, with a maximum width at the 7th rib. Here, we reassess the anatomical position of the thoracic vertebrae and ribs of RdM, evaluating previous observations using a combination of traditional measurements and 3D geometric morphometrics. A morphological assessment of the most complete ribs (7, 9, 10 and 11) reveals marked differences between the ribs of RdM and those of modern human children. These differences include less curvature of the shaft in cranial view, more vertically oriented and straighter (i.e., less sinuous, with less torsion) shafts in external view. At least for ribs 9–11, the shaft portion sternal to the posterior angle is also longer. In some instances, these differences are similar to those present in adult Neandertals, suggesting that the Neandertal thorax was distinct from that of* H. sapiens *since infancy. This study reinforces the idea that the size and shape of the individual elements (the ribs and vertebrae) provide information about the distinctiveness of the entire thorax.*

Keywords - *Spine, Thorax, Geometric morphometrics, Sliding semilandmarks, Ontogeny, Development.*

Introduction

The 3D virtual reconstruction of the thorax of the adult Neandertal Kebara 2 (K2; Gómez-Olivencia et al. 2018) provided a deeper understanding of the significant differences found in the costal skeleton and thoracic vertebrae of Neandertals compared to modern humans (Franciscus and Churchill 2002; Weinstein 2008; Gómez-Olivencia et al. 2009, 2019; García-Martínez et al. 2014, 2017, 2018b; Bastir et al. 2015, 2017; Gómez-Olivencia 2015). Compared to modern humans, the Kebara 2 thorax shows significant differences in shape, as it is absolutely wider, concurrent with a wide pelvis, and shows a more invaginated spine, likely

related to the position of the sacrum within the pelvis. Additionally, the ribs are more horizontally oriented in lateral view (Gómez-Olivencia et al. 2018). These overall differences are in addition to, and the result of, those found in the individual ribs and vertebrae, both in K2 and other Neandertal specimens. These differences include a longer arc length and a greater distance between the articular tubercle and the iliocostal line in the middle ribs (tubercle-iliocostalis distance; TID), the larger size of the articular tubercles in the lower ribs, differences in the overall shaft curvature in some ribs (e.g., the 1st rib is less curved), larger shaft dimensions in certain areas (e.g., at the posterior angle in the upper ribs and at the sternal end in the middle ribs), and the more dorsal orientation of the transverse processes of the mid-thoracic vertebrae (Gómez-Olivencia et al. 2009, 2019; Bastir et al. 2015, 2017; Gómez-Olivencia 2015; García-Martínez et al. 2017). Surprisingly, despite these morphological differences, the overall size of the thorax (using the geometric mean as a size proxy) is not different for the K2 individual compared to modern humans, due to a smaller overall cranio-caudal dimension of the reconstructed thoracic spine in K2 (Gómez-Olivencia et al. 2018). In lateral view, the K2 thorax reconstruction shows more horizontal ribs than modern humans, which likely constrained rib elevation (via bucket-handle movements), and has a wider lower thorax when compared to modern humans (Gómez-Olivencia et al. 2018). In modern humans, rib cages that are wider in absolute and relative terms in their lower half result in larger respiratory capacity during inspiration (García-Martínez et al. 2016). The presence of larger articular tubercles on the lower ribs of Neandertals may indicate a larger involvement of the lower thorax in breathing (Franciscus and Churchill 2002; Gómez-Olivencia et al. 2019). Indeed, the work of Gómez-Olivencia et al. (2018) suggests that Neandertals may have had a breathing mechanism that differed somewhat from that of modern humans, relying relatively more on diaphragm contraction. This interpretation of the Neandertal thorax anatomy would be consistent with other approaches to calculating the total lung capacity (TLC) of Neandertals, which are based on the correlation between TLC and costal size, that have provided estimates of larger capacities for Neandertals when compared to modern humans of the same sex (García-Martínez et al. 2018c). Despite the presence of some anomalies in the spine and costal skeleton of the Kebara 2 skeleton (Duday and Arensburg 1991; Been et al. 2017; García-Martínez et al. 2018a), studies of less complete individuals (e.g., La Chapelle-aux-Saints 1, Regourdou 1, Shanidar 3) suggest that K2 is not an outlier (Franciscus and Churchill 2002; Gómez-Olivencia et al. 2009, 2013, 2019; Gómez-Olivencia 2015). Nevertheless, additional and more complete Neandertal costal remains are needed in order to better understand Neandertal variation.

Apart from their important physiological implications, the size and shape of the thorax also play a central role in debates surrounding the evolution of body size and shape within the genus *Homo* (Arsuaga et al. 1999, 2015; Carretero et al. 2004; Bonmatí et al. 2010; Holliday 2012; Bastir et al. 2020). In this context, the absolutely wide thorax of Neandertals has been linked to an absolutely wider body frame (Franciscus and Churchill 2002; Gómez-Olivencia et al. 2009, 2018), which has been proposed as a primitive trait within genus *Homo* (Arsuaga et al. 1999, 2015). Indeed, the recent reconstruction of the thorax of the juvenile *Homo erectus* individual KNM-WT 15000 shows it to be absolutely wider than that of modern humans of a similar age, and similar to that of modern human adults (Bastir et al. 2020). However, the situation is more complicated than it seems. Despite having wider pelvises than modern humans in absolute terms, Neandertals may have had slightly narrower bodies than their Middle Pleistocene ancestors (Rak 1991; Rosenberg et al. 2006; Bonmatí et al. 2010; Trinkaus 2011). However, this observation is based on a very limited sample: the bi-iliac breadth of two Middle Pleistocene pelves, Jinniushan (female; 344 [327-361] mm) and Sima de los Huesos-Pelvis 1 (male; 335 mm), which show larger dimensions than the

estimations calculated for two Neandertal pelves, comprising Kebara 2 (Male; 313 mm) and La Chapelle-aux-Saints 1 (Male; 292 mm). Therefore, assessing body-width trends within the Neandertal lineage would require additional fossil specimens. In this context, studying the ontogeny of the Neandertal thorax as a whole reveals differences in size and shape between Neandertal individuals and similar age groups in *H. sapiens* (García-Martínez et al. 2020). This is consistent with evidence suggesting that distinct Neandertal thoracic morphology is exclusive to the Neandertal lineage or is mostly primitive within genus *Homo*.

Several relatively complete subadult Neandertal costal skeletons have been found, including published (Dederiyeh 1 and 2; Roc de Marsal) and unpublished (Mezmaiskaya; Le Moustier 2) individuals. The ribs of Dederiyeh 1 have been characterised as relatively robust, with large and triangular cross sections, wide and shallow costal grooves, and similar in curvature to *H. sapiens* infants or even more strongly curved in the lower ribs (Kondo and Dodo 2003). In contrast, the ribs of the individual from Roc de Marsal (RdM), have been described as gracile (*une robustesse peu importante*), with short necks, a large radius of curvature and a pronounced anterior flare, which would be indicative of a thorax that was developed antero-posteriorly, reaching its maximum width at the 7th rib (Madre-Dupouy 1992). The RdM ribs also exhibit a marked torsion straightening the outer face, especially in the middle of the rib, and a wide rib groove (Madre-Dupouy 1992). Regarding the curvature, Kondo and Dodo (2003) attributed the apparent inconsistency between the Dederiyeh and RdM specimens to the wide variation present in the morphology of adult Neandertal ribs.

More recently, 3D virtual reconstructions of the thoraxes of immature Neandertals (Mezmaiskaya 1, Le Moustier 2, Dederiyeh, and RdM) enabled us to assess whether the differences observed in the Neandertal adult thorax as a whole were already present at birth and in the early stages of development of this human group (García-Martínez et al. 2020). García-Martínez et al. (2020) indicated that the comparatively antero-posteriorly deep and cranio-caudally short ribcage of Neandertals was already present at birth. The virtual reconstruction of the RdM specimen was possible due to the amendment of the anatomical position of several vertebrae and ribs of this individual. In this study, we present the anatomical criteria for this reassessment and provide a detailed analytical study of selected RdM vertebrae and ribs. We also aim to test whether the distinct overall Neandertal thoracic morphology is related to morphological differences present on the individual costal elements (and vertebrae). Additionally, discrepancies previously detected between the morphology of the RdM ribs and those of the Dederiyeh specimen will be discussed. To that end, firstly, we reassess the anatomical position of the ribs and vertebrae of the RdM Neandertal infant and compare our findings with those previously published (Madre-Dupouy 1992). Secondly, we provide a complete metric assessment of the vertebral and rib fragments, which are necessary in the serial identification of the vertebrae and ribs and also to compare to modern humans. Thirdly, we conduct a comparative morphometric analysis of the most complete ribs using 3D geometric morphometrics. Finally, we will compare selected morphological traits of the infant RdM vertebrae and ribs with those of Neandertal adults, in order to evaluate whether some of the distinct Neandertal features present in the adult spine and thorax are already present in the infants, and discuss these results within the more general Neandertal ontogenetic assessment provided by García-Martínez et al. (2020).

Materials and methods

The Roc de Marsal (RdM) skeleton

The Neandertal infant from RdM was found in 1961 in a small cave near Campagne-de-Buge (Dordogne, France) during the excavations performed by J. Lafille from 1953 until his death in 1971 (Lafille 1961; Bordes and Lafille 1962;

Turq 1989); it constitutes one of the most complete Western European immature Neandertals. Sandgathe et al. (2011) provide a complete description of the finding of the RdM individual. An entire block encompassing the RdM remains was removed from the site and transferred to the Institut de Paléontologie Humaine (Paris), where Jean Piveteau removed the human remains from the sediment (Sandgathe et al. 2011).

Based on modern human standards, Bayle et al. (2009) estimated an age-at-death interval of 2.5-3 years for this individual. However, neither the deciduous nor the permanent mandibular sequences displayed by the RdM infant were found in the reference samples used by Bayle et al. (2009), as the first molars are relatively advanced and the incisors relatively delayed in terms of their mineralization stages.

The thoracic spine and costal remains of Roc de Marsal

We studied the original RdM skeleton housed at Musée National de Préhistoire (MNP; Les Eyzies-de-Tayac-Sireuil, France). The thoracic spine of RdM comprises the partial (n = 3) and complete (n = 9) neural arches of all 12 thoracic vertebrae, as well as four partial and four complete vertebral bodies. The neural arches and the vertebral bodies were treated separately as they are not fused, and in some instances (e.g., T5 and T6) it is still possible to see the fusion line between the two halves of the neural arch, each of which constitutes a primary ossification center. We cross-checked whether the most complete vertebral bodies could be articulated with the neural arches. All these vertebral remains were "virtually" labelled following Madre-Dupouy's (1992) Figure 68 (Supplementary Material Fig. S1). The costal skeleton of RdM comprises nine rib or rib fragments from the left side. From the right side, 11 rib or rib fragments are preserved, plus a fossil specimen that preserves three shaft fragments from three different ribs. Six additional rib shaft fragments are associated with the RdM skeleton, though their fragmentary status does not allow for their precise anatomical determination (Supplementary Material Fig. S2). Finally, it should be noted that casts were made of the vertebrae at some point to obtain replicas and as a consequence, the original fossils are more fragmentary when compared to the original publication (Madre-Dupouy 1992).

Anatomical determination of vertebrae and ribs

The sequential anatomic determination of the RdM thoracic vertebrae followed known diagnostic morphometric features present in adult Neandertal individuals, e.g., distinctive morphology and more lateral orientation of the transverse processes in the upper-most thoracic vertebrae, high proportions of absence or near absence of transverse process and change of facet orientation of the last thoracic vertebra, differences in orientation of the spinous process from more horizontal in the cranialmost and caudalmost thoracic vertebrae, and more caudally inclined in the mid-thoracic spine (e.g., Gómez-Olivencia et al. 2013). The sequential anatomic determination of the vertebral bodies, followed known features such as changes in shape from the upper-most (T1-T2) to subsequent vertebrae and the general increase in size from cranial to caudal. The anatomic determination of ribs 2-12 (rib one is missing) followed criteria published elsewhere (Mann 1993; Dudar 1993; Cirillo and Henneberg 2012), especially the sequential increase in general size towards ribs 6-7 and subsequent decrease towards lower thorax, and the increase in tuberculo-iliocostalis line distance from the 3rd to the 9th ribs. Additionally, the antimeres proposed by Madre-Dupouy (1992) were assessed in order to determine if they were symmetric. The metric assessment of the vertebrae and ribs followed the standards found in the literature (e.g., Franciscus and Churchill 2002; Gómez-Olivencia et al. 2010, 2013).

3D geometric morphometric analysis of the most complete ribs

The comparative 3D geometric morphometric analysis was performed on the most complete ribs (ribs 9R, 10L, and 11L) of RdM. The 3D geometric morphometric analyses were restricted to ribs 9, 10 and 11 because these elements represent the best-preserved thoracic remains in the RdM

assemblage. These ribs preserve the complete morphology from the costal tubercle to the sternal end and show no fractures, post-depositional deformation, or taphonomic damage that could alter their original curvature or spatial orientation. Importantly, no virtual or physical reconstruction was required prior to landmark and semilandmark digitization. Other ribs from the assemblage were not included in the morphometric analyses because they are fragmentary or affected by preservation-related alterations that preclude reliable quantification of their original shape. These ribs were scanned using an Artec Spider 3D scanner (https://www.artec3d.com/). The 9th rib was compared to immature *Homo sapiens* since there is no complete 9th ribs preserved for adult Neandertals. The 10th and 11th ribs were compared to two adult Neandertals (Kebara 2 and Regourdou 1), and both adult and immature modern *Homo sapiens*. The complete 11th rib from the right side of the Regourdou 1 adult Neandertal individual was used (Gómez-Olivencia et al. 2019). It was CT-scanned at the AST-RX platform ("Accès Scientifique à la Tomographie à Rayons X") using the microfocus tube of the micro-CT scanner "v|tome|x L 240" (GE Sensing & Inspection Technologies Phoenix X|ray) at a resolution of 87.67 µm and a 3D object was derived using AvizoLite software. The 10th rib from the right side and the 11th rib from the left side of the Kebara 2 individual were also used. The scans of the ribs of this individual were made with a medical CT scan at Mount Carmel Medical Center, Haifa (voxel size: 0.598958 × 0.598958 × 0.5 mm), and 3D objects were derived from all scans using AvizoLite v.9 software. The modern human comparative sample comprises a total of 16 individuals, including 10 adults (all >20 years; 5 males and 5 females) and 6 infants (ages ranging from 1.2 to 3.2 years, mean age 2.4 years; 2 males and 4 females). All individuals were classified as adult or infant based on documented chronological age. The comparative modern human children were specifically selected to closely match the chronological age of the Roc de Marsal individual. Only ribs preserving complete morphology and suitable for landmark and semilandmark digitization were included in the 3D geometric morphometric analyses. The modern human subadult and adult modern human data were gathered from Computed tomography (CT) obtained from subjects that were scanned previously in supine position and maximum expiration for medical reasons unrelated to this study (retrospective) at the Medizinischen Universität Innsbruck (Austria) and Hospital de la Paz (Madrid, Spain). No obvious pathologies affected skeletal thoracic form in any of these individuals. Consent was given by the respective ethical committees to use these CT-data for research purposes and all modern human CT-data were anonymized to comply with the Helsinki declaration (Goodyear et al. 2007).

We segmented ribs 9, 10, and 11 from each thorax, using a semi-automatic segmentation protocol of DICOM images, employing the software 3D slicer v. 4.11 (https://www.slicer.org/; Fedorov et al. 2012) and the final 3D models were imported into Viewbox4 software (www.dhal.com). Landmarks and sliding semilandmarks (Gunz et al. 2005; Bastir et al. 2019) were located on the 3D rib models following the protocol of García-Martínez et al. (2017). Thus, the morphology of the ribs 9 and 10 is described by 61 homologous 3D landmarks and sliding semilandmarks on each rib (Supplementary Material Fig. S3), whereas 44 landmarks and sliding semilandmarks were used to describe the morphology of ribs 11 (Supplementary Material Fig. S4). These protocols were applied to both the fossil and comparative samples (total n = 44 ribs) by collecting information from the entire rib, i.e., from the rib head to the distal end.

For the 3D analyses, size and shape data were obtained through generalized Procrustes analysis (GPA) of this landmark data set (Zelditch et al. 2012). Rib size was quantified as centroid size, which is defined by the square root of the sum of squared distances of a set of landmarks from their centroid (Bookstein 1991). Patterns of shape variation along the sample were studied via principal component analysis (PCA) in Procrustes shape space (Zelditch et al. 2012). Ordinations were calculated and shape differences of the surface associated with variations along the PC axes were visualized using EVAN Toolkit (version 1.71; http://

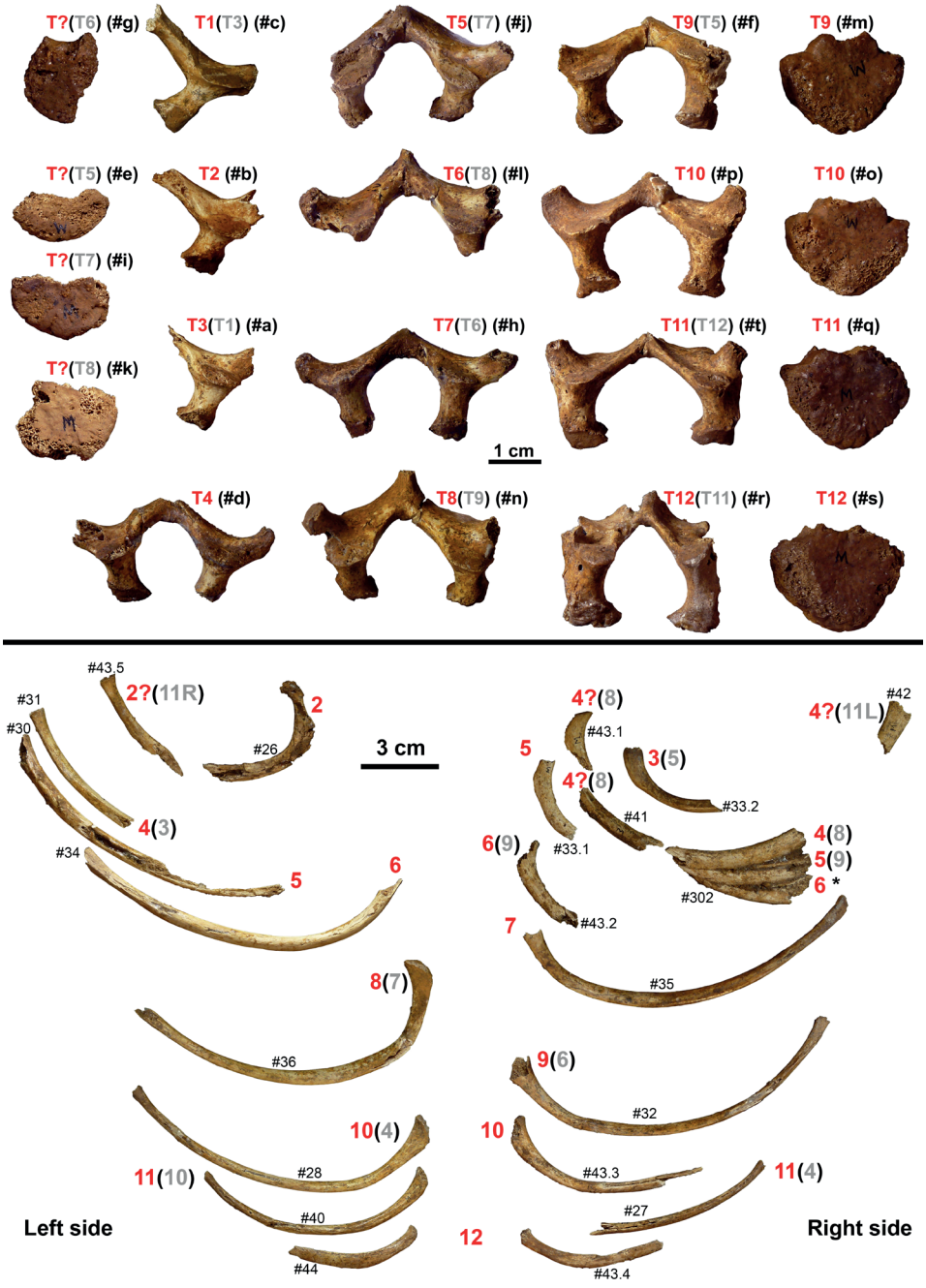

Fig. 1 - Cranial view of the thoracic vertebrae and ribs of Roc de Marsal 1 Neandertal individual showing the anatomical position and the virtual label (vertebrae; Supplementary Material Fig. S1) or the inventory number of the Musée National de Préhistoire (ribs). Numbers in parentheses indicate the cases in which the anatomical position assigned by Madre-Dupouy (1992) differ from ours.

Tab. 1 - Preservation of the neural arches of the thoracic vertebrae of the Roc de Marsal Neandertal infant[a].

SERIAL POSITION	VIRTUAL LABEL[B]	NUMBER OF FRAGMENTS THAT CONSTITUTE THIS SPECIMEN	PEDICLE (R/L)	TRANSVERSE PROCESS (R/L)	UPPER ARTICULAR FACET (R/L)	LOWER ARTICULAR FACET (R/L)	LAMINA (R/L)	SPINOUS PROCESS
T1	#c	1	-/C	-/C	-/C	-/P	-/C	-
T2	#b	1	-/C	-/P	-/C	-/C	-/P	-
T3	#a	1	-/C	-/P	-/C	-/C	-/P	-
T4	#d	3	C/P	P/C	P/C	C/C	P/C	-
T5	#j	3	P/C	-/C	C/C	C/C	P/C	-
T6	#l	2	-/P	C/-	C/C	C/C	C/P	P
T7	#h	2	P/C	C/C	P/C	C/C	C/C	-
T8	#n	2	C/C	C/-	C/C	C/C	C/C	C
T9	#f	2	C/C	P/-	C/P	P/C	P/C	-
T10	#o	3	C/C	C/C	C/C	C/C	C/C	P
T11	#t	3	C/C	C/C	C/C	C/C	C/C	-
T12	#r	4	C/C	P/-	C/C	C/C	C/C	P

[a] C= complete or nearly complete; P=partially preserved. R = right; L = left. [b] Based on the order in which they were published by Madre-Dupouy, 1992 (Supplementary Material Fig. S1).

www.evan-society.org/). For statistical comparison between modern humans and the RdM specimen, a pooled dataset including the 9th and 10th ribs was constructed. Pooling was possible because both rib levels were digitized using the same landmark and semilandmark configuration and followed an identical digital acquisition and sliding protocol. Differences between groups were evaluated using a Procrustes ANOVA implemented in MorphoJ, based on Procrustes-aligned landmark coordinates obtained after Generalized Procrustes Analysis. Centroid size was first compared between groups using a univariate ANOVA to evaluate potential size differences. The 11th rib was excluded from group-level statistical testing because it was digitized using a different landmark configuration and is represented by a single Neandertal specimen only (n = 1), which prevents reliable estimation of within-group variance.

Traditional morphometric assessment of the overall curvature of ribs 10 and 11

To compare the overall curvature of the RdM ribs 10 and 11 to modern human children and to assess this curvature in adult Neandertals bivariate plots were used using the head/tubercle-ventral arc (HVA/TVA) vs. head/tubercle-ventral chord (HVC/TVC) following Gómez-Olivencia et al. (2010).

Results

Revised anatomical position of the vertebrae

Synthetic inventories of the neural arch fragments and vertebral bodies are shown in Tables 1-2 and the raw dimensions of the neural arches are presented in Supplementary Material Table S1. Comparison of our results with those previously published can be found in Figure 1.

***Tab. 2** - Preservation of the vertebral bodies of the thoracic vertebrae of the Roc de Marsal Neandertal infant[a].*

VIRTUAL LABEL	AMENDED SERIAL POSITION	PREVIOUS SERIAL POSITION[b]	PRESERVATION
#g	T?	T6	P
#e	T?	T5	P
#i	T?	T7	P
#k	T?	T8	P
#m	T9	T9	C
#o	T10	T10	C
#q	T11	T11	C
#s	T12	T12	C

[a] C= complete or nearly complete; P=partially preserved.
[b] According to Madre-Dupouy, 1992.

The anatomical order of 75% (9 of 12) of the neural arches of the thoracic vertebrae has been amended. To seriate the vertebrae we relied on both morphological description and metric observations, including observations of the size of the pedicle, size and orientation of the transverse process, height of the neural arch (from the cranial-most point of the upper articular facets to the caudal-most point of the lower articular facets; i.e., bi-articular diameter), height of the lamina, position of the transitional vertebra (the vertebra in which the orientation of the facet changes from transversal to para-sagittal), and the articular congruence between vertebrae. Uppermost thoracic vertebrae have more "cervical-like" neural arches, with lower values of bi-articular diameter, which increase caudally (Supplementary Material Tab. S1 and Fig. 2), and the pedicles become thinner and taller towards mid-thoracic vertebrae and larger in both height and thickness towards the caudal-most thoracic vertebrae (Supplementary Material Tab. S1). The distance between the cranial-most point of the upper articular facets and the union of the laminae also increase caudally, and the union of the laminae display a more accentuated V shape in dorsal view (Supplementary Material Fig. S5; compare with Madre-Dupouy 1992: Figure 70). The superior articular facet appears to be positioned at approximately the same height as the transverse process at the T1 vertebra but is positioned more cranially than the transverse process towards the mid-thoracic spine, while the transverse process is shifted caudally relative to the pedicle (Supplementary Material Fig. S5). The lowermost thoracic vertebrae show more robust pedicles with large facets for the articulation of the rib and more dorsally oriented transverse processes which become smaller towards the lower-most vertebrae. Additionally, we have identified the transitional vertebra (i.e., the vertebra marking the transition in articular facet orientation from a roughly transverse orientation (typical of thoracic vertebrae to a more para-sagittal orientation, typical of lumbar vertebrae; Williams 2012; Williams et al. 2016), but no rib-bearing post-transitional vertebra. Thus, in this individual the transitional vertebra is the last rib-bearing vertebra. Finally, despite some of the neural arches being incomplete, all 12 thoracic vertebrae are represented, which facilitates seriation.

Here we describe the details we used to amend the anatomical position of the neural arches of RdM (from T1 to T12):

T1. (previously described as a T3). This fragment shows the smallest bi-articular diameter (more cervical-like) and a lateral orientation of the transverse process, which corresponds to a T1. Additionally, the superior articular facets are located approximately at the same height at the transverse process, as in adult T1s.

T2. The anatomical position of this fossil is unchanged.

T3. (previously described as a T1). The position of the superior articular facets regarding the transverse processes is intermediate between the T2 and T4 vertebrae, as is the bi-articular diameter.

T4. The anatomical position of this fossil is unchanged.

T5 to T8. These vertebrae have been seriated following a morphological cline taking into

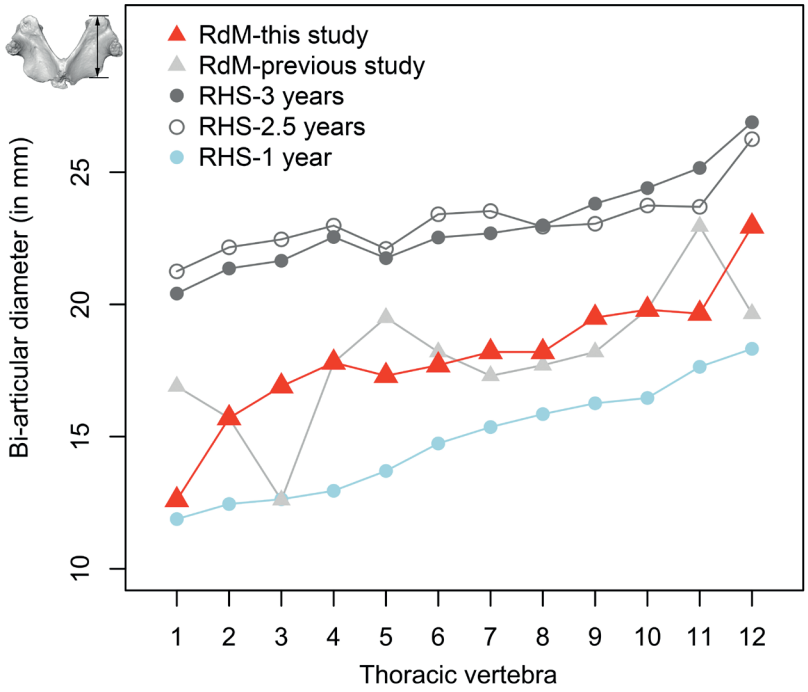

***Fig. 2** - Univariate representation of the bi-articular diameter across the thoracic spine of Roc de Marsal (both the previous and current anatomical determinations) compared to three recent* **H. sapiens** *(RHS). For the RdM individual, when possible the average values between the left and right sides have been used (Supplementary Material Tab. S1).*

account the robusticity of the pedicle, the bi-articular diameter and the increased distance between the articular facets and union of the laminae.

T9. (previously described as a T5). This vertebra has slightly larger pedicles than T8, and its bi-articular diameter is larger than T8. Additionally, this specimen refits with #m, the vertebral body assigned to a T9 (Fig. 1).

T10. The anatomical position of this fossil is unchanged.

T11. (previously a T12). This vertebra is morphologically intermediate between T10 and T12, with smaller and slightly more dorsally oriented transverse processes than T10 and a V-shaped union of the laminae. The laminae are also thinner than T10 but not as much as in T12 (Tab. 3).

T12. (previously a T11). This neural arch has the largest value in cranio-caudal direction (i.e., bi-articular diameter; Fig. 2) and it is the transitional vertebra.

The four most complete vertebral bodies correspond to T9–T12, based on their general size increase from cranial to caudal, which is consistent with previous anatomical assessment (Madre-Dupouy 1992). We believe that the four incomplete vertebral bodies, previously published as T5-T8, are not sufficiently complete to allow us to assess their anatomical position beyond their T1-T8 position.

Revised anatomical position of the ribs

Table 3 provides an inventory of the costal remains of RdM; Supplementary Material Tables S2 and S3 describe metrically the RdM ribs. The

Tab. 3 - General inventory of the preservation status of costal remains of the Roc de Marsal Neandertal infant[a-b].

SERIAL POSITION	SIDE	LABELS	HEAD	NECK	TUBERCLE	SHAFT	POSTERIOR ANGLE	SHAFT	STERNAL END
1	R					N/A	N/A		
	L					N/A	N/A		
2	R					N/A	N/A		
	L	#26, #43.5(?)	C	C	C	N/A	N/A	P	C
3	R	#33.2			P	C	C	P	
	L								
4	R	#43.1, #41(?), #302, #42(?)	P	C	C			P	
	L	#31						P	C
5	R	#33.1, #302			C	C	C	P	
	L	#30						P	P
6	R	#43.2, #302			P	C	P	P	
	L	#34				P	C	C	P
7	R	#35				C	C	C	P
	L								
8	R								
	L	#36	C	C	C	C	C	C	
9	R	#32		P	C	C	C	C	P
	L								
10	R	#43.3							
	L	#28	C	C	C	C	C	C	C
11	R	#27		N/A	N/A			P	
	L	#40	C	N/A	N/A	C	C	C	P
12	R	#43.4	P	N/A	N/A	C	C	C	
	L	#44	C	N/A	N/A	C	C	C	

[a]C = complete or largely preserved; P = partially preserved; N/A = not applicable. [b]Six additional rib shaft fragments, for which the determination of the anatomical seriation was not possible, are not listed here (Supplementary Material Fig. S2).

anatomical sequence of 66% of the ribs (14 of 21 specimens) has been amended and in some cases the differences are striking, including two ribs for which we propose a different side. Due to the incompleteness of some of the ribs, some of the proposed anatomical positions remain tentative. Moreover, because not all the ribs are preserved, their sequencing is more difficult than

in the case of the vertebrae. Thus, we tried to find potential antimeres and sequence the ribs taking into account known morphological features, such as the increase from cranial to caudal of the distance between the tubercle of the rib and the posterior angle (tuberculo-iliocostalis line distance) from the 3rd to the 9th ribs, the increase in absolute rib length (from rib tubercle to sternal end) from rib 1 to mid-thorax and its subsequent decrease, the more diagonal orientation of the shaft in upper thoracic ribs, and the presence of blade-like shafts in the lower ribs, among others (Mann 1993; Dudar 1993; Cirillo and Henneberg 2012).

Here we describe the details of our approach to amend the anatomical sequence of the ribs:

Rib 1. There are no first rib remains.

Rib 2. Right. There are no remains of the right second rib.
Left. The anatomical determination of #26 has not changed (Supplementary Material Tab. S2). Additionally, we have identified #43.5 as a probable left second rib based on the flatness of the shaft. This rib was previously determined as an 11R, but the lack of curvature and the external morphology is not consistent with this determination.

Rib 3. Right. #33.2 is classified as a 3R due to the small distance between the tubercle and the posterior angle.
Left. There are no 3L remains.

Rib 4. Right. We have tentatively classified both #43.1 and #42 as part of the 4R rib. #43.1 was previously classified as an 8th rib, but comparison with #36 suggested that it belonged to a more cranially-positioned rib. The preserved anatomical region of #43.1 (partial head, neck and tubercle (Tab. 3 and Fig. 1) is also present in other ribs from the right side, and therefore we consider it likely to have belonged to a 4th rib. #42, previously classified as an 11th rib from the left side, is the sternal end of a rib. When compared with the preserved sternal ends of the lower-most ribs and the ribs from the left side, its size is similar to #31 (classified here as a 4L). The shaft fragment #41 was also tentatively assigned to a 4R.
Left. We shifted the anatomical position of #31, a shaft fragment preserving the sternal end, from a 3R, as it is morphologically closer to #30 (5L) than to #43.5 (2?L).

Rib 5. Right. The anatomical determination of this fossil is unchanged.
Left. The anatomical determination of this fossil is unchanged.

Rib 6. Right. The overall morphology of #43.2 is more similar to #34 and has a shorter distance between the tubercle and the posterior angle than #32, which indicates that that #43.2 is located more cranially than #32.
Left. The anatomical determination of this fossil is unchanged.
The fossil labelled #302 was previously published as an 8-9th rib. This fossil comprises the shafts of three different ribs. Based on the new determination of other elements we consider it more likely that this fossil and the shaft fragments represented are located more cranially than #35 (7R), and therefore they represent shaft fragments from the 4th, 5th and 6th ribs from the right side.

Rib 7. Right. The anatomical determination of this fossil is unchanged.
Left. There are no 7L remains.

Rib 8. Right. There are no 8R remains.
Left. Based on the difference in the curvature in cranial view #36 is not the antimere of #35 (7R). Additionally, the distance between the tubercle and the posterior angle is smaller than #32 (9R), which is consistent with its classification as an 8th rib. Note also that we believe the curvature of #36 is due to an incorrect reconstruction which resulted in an exaggerated curvature of this rib.

Rib 9. Right. #32 was previously classified as a 6R, but it is smaller than #35 and the

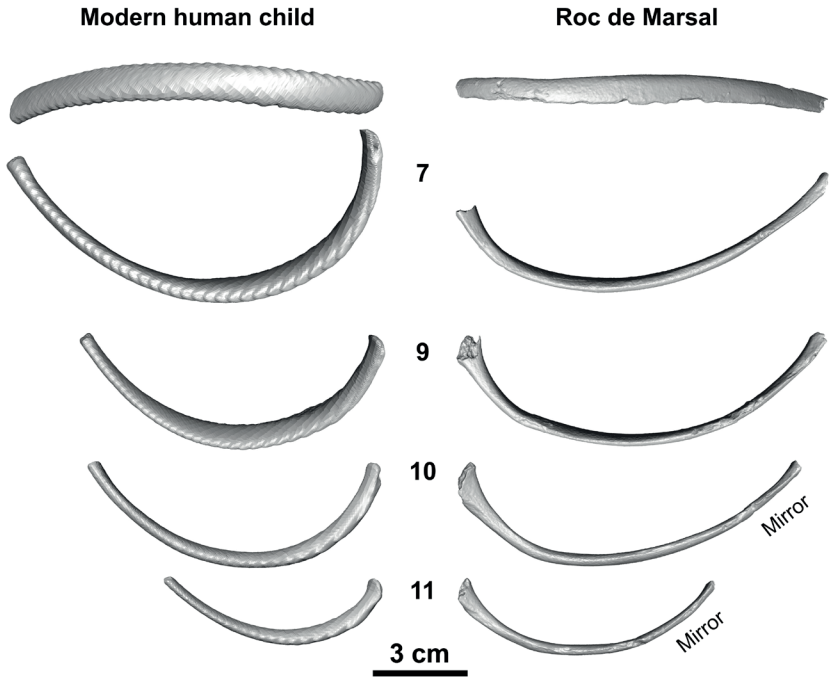

***Fig. 3** - Comparison of the Roc de Marsal (RdM) most complete mid-lower ribs to the oldest modern human individual of our sample. RdM shows some differences, such as a less curvature of the ribs, a more horizontal (less sinuous) shaft in rib 7 as observed on external view, and more vertically oriented rib shaft. Ribs 9 and 10 from RdM show some differences in the robusticity of the head.*

distance between the tubercle and the posterior angle suggested a more caudal position, caudal to #36 (8R) but cranial to #43.3 (10R) and #28 (10L).

Left. There are no 9L remains.

Rib 10. Right. The anatomical determination of this fossil (#43.3) is unchanged. This rib has been reconstructed and is now more complete than when it was first published.

Left. #28 (complete 10L) is the antimere of #43.3 (10R). It cannot be a 4th, as previously proposed, as 4th ribs are more curved, show a different orientation of the shaft (more diagonal, with the interior part of the mid-shaft facing a roughly medial-caudal direction, while mid-thoracic ribs are more vertically oriented and lowermost ribs show a more diagonal orientation, but in the opposite direction, with the interior part of the mid-shaft facing a roughly medial-cranial direction) and shorter distances between the vertebral end and the posterior angle.

Rib 11. Right. #27 was previously classified as a 4th rib, but we would expect a shaft that is more curved and oriented more diagonally from a cranial-internal to a caudal external direction. Thus, we deem to be morphologically compatible to be the antimere of #40.

Left. #40 (previously classified as a 10th rib) shows an overall size (especially in the head and all the vertebral end of the rib) intermediate between the 10R and the 12th ribs.

Rib 12. The anatomical position of both ribs, which are reasonably complete, has not changed.

Tab. 4 - Comparisons of rib thickness/height index[a] at the posterior angle.

	ROC DE MARSAL		DEDERIYEH 1[b]		MODERN HUMANS[b]			
	LEFT	RIGHT	LEFT	RIGHT	MEDIAN	MINIMUM	MAXIMUM	N
Rib 2			61.1	50.7	60.3	50.8	71.4	9
Rib 3			61.8	52.9	57.1	50.0	72.7	9
Rib 4			67.7	53.3	68.0	53.0	76.0	9
Rib 5		75.0	66.7	56.3	76.5	67.3	82.6	9
Rib 6	70.3		67.1	61.8	71.7	65.5	80.6	9
Rib 8			60.7	57.1[c]	60.6	55.6	66.1	9
Rib 9		55.1	59.5		51.7	46.0	65.6	9
Rib 10	53.2	52.0	47.5	50.0	54.3	40.2	61.9	8
Rib 11	58.2		66.7	63.3				

[a] Thickness/height index = SMnD/SMxD × 100. [b] Kondo and Dodo (2003). [c] Identified as an 8th or 9th rib by Kondo and Dodo (2003).

There are six additional shaft specimens for which the anatomical position was not determined due to their incompleteness (Supplementary Material Fig. S2). Rib #42 (according to the labelling of the MNP) seems to be less complete than when it was first published by Madre-Dupouy (1992). In regard to the three shafts that appeared together (#302), it seems that one of them was not included in the inventory provided by Madre-Dupouy (1992). Finally, we have been able to refit a rib fragment and, thus, rib #43.3 (10R) is now more complete.

Comparative morphological and metric assessment of the RdM individual

Morphological assessment. Direct comparison between the most complete ribs (7, 9, 10, 11) of RdM with the oldest (and largest) child of our comparative sample illustrates that RdM ribs appear to be systematically less curved than the modern human specimen, and, for ribs 9–11, the most complete ones, RdM displays longer ribs (Fig. 3). The relative position of the posterior angle also appears different in RdM: the longer shafts of the RdM ribs appear less proportionately distributed such that the shaft sternal to the posterior angle appears longer than in modern humans. We observe some additional differences, such as a more vertical orientation of the RdM rib shafts; i.e., the internal surface of the modern human ribs appear to be oriented slightly more cranially and in external view the shafts appear straighter. Regarding the robusticity (thickness/height) index at the posterior angle, the RdM ribs are similar to a small modern human sample (Tab. 4).

Metric comparisons. The centroid size (CS) of RdM ribs 9-11 showed larger values (CS_9 = 340.02, CS_{10} = 318.59, CS_{11} = 195.14) than the average of modern human infants (CS_9 = 338.5., CS_{10} = 298.27; CS_{11}=187.18). The principal component analysis (PCA) of shape variation on ribs 9 and 10 showed that PC1 vs. PC2 projection polarizes morphological variation regarding anatomical position in PC1 (69.34% of variation explained) where 9th ribs plot towards the positive values and 10th ribs towards the negative ones. In addition, PC2 (11.51% of variance explained) separates modern humans (more positive scores) from the RdM Neandertal (more negative scores), which indicate less curved ribs, with cranio-caudally smaller shafts in the RdM individual. Additionally,

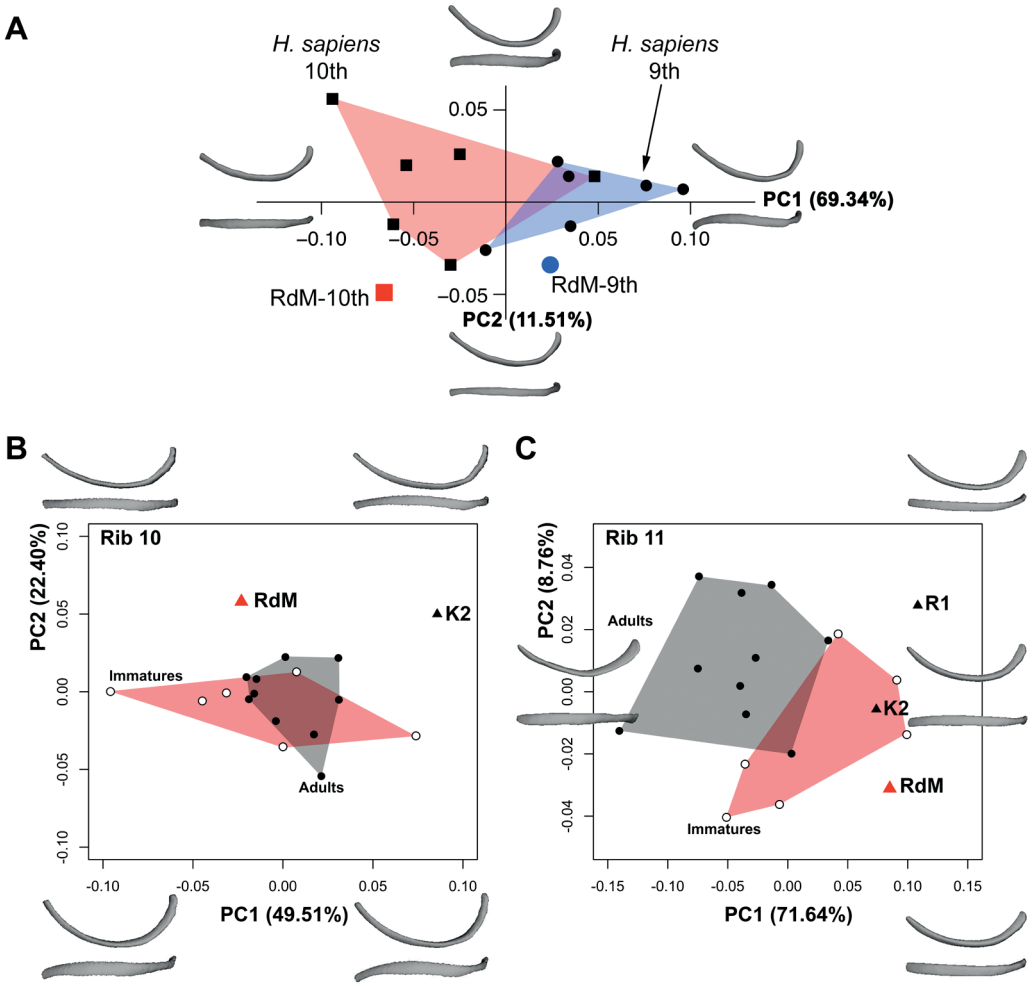

Fig. 4 - A) Principal component (PC) shape analysis of 9th (solid circles) and 10th (solid squares) ribs of Roc de Marsal (RdM) individual (red and blue) compared to a modern human subadult comparative sample (black). The blue polygon represents the morphospace occupied by the 9th ribs of the subadult modern human comparative sample, and the red polygon represents the morphospace occupied by the 10th ribs of the same sample. B and C) Principal component (PC) shape analysis of ribs 10 (B) and 11 (C) comparing RdM infant to the Kebara 2 (K2; left panel) and Regourdou 1 (R1; right panel) adult Neandertals, and to immature and adult modern human samples. Scatterplots depict the first two principal components.

the RdM ribs display relatively longer shaft portions sternal to the posterior angle (Fig. 4A). The Procrustes ANOVA on shape showed highly significant differences between modern humans and the Roc de Marsal Neandertal ribs pooled 9th and 10th ribs (F = 1.36, p = 0.0017). In contrast, the analysis of centroid size for the pooled 9th and 10th rib dataset revealed no significant differences between modern humans and the Roc de Marsal specimen (F = 0.01, p = 0.905), indicating that both groups are comparable in overall rib size. Therefore, the observed morphological differences reflect genuine shape variation rather than size-related effects.

In the second and third shape analyses we have compared RdM ribs 10 and 11, respectively, to other adult Neandertal ribs as well as to both immature and adult modern human individuals (Fig. 4). In the case of rib 10, the most positive values of PC1 (49.51% of the variation explained; Fig. 4B) represent more sinuous ribs in lateral view. In this PC we cannot distinguish a general ontogenetic pattern within modern humans, as modern human adults are approximately within the range of variation of immature individuals. It should be noted that Kebara 2 (K2) falls well outside the range of variation of our modern adult comparative sample (n = 10), while the RdM infant shows a value similar to the mean of modern immature individuals. PC2 (22.4% of the variation explained) separates Neandertals, with overall less curved ribs in cranial view, and cranio-caudally less developed shafts in lateral view, from modern humans, who show overall more curved ribs in cranial view with cranio-caudally more developed shafts in lateral view. In the case of rib 11 (Fig. 4C), modern adults show lower values of PC1 (71.64% of the variation explained) and, to a lesser extent, higher values of PC2 (8.76% of the variation explained) than immature individuals. This is related to an increase of curvature of the rib in cranial view, to a less vertical orientation of the shaft and to a more central position of the posterior angle within the shaft. Neandertals display larger values of PC1 than modern humans, and distribute closer to the modern human immatures, though above their mean or outside their range of variation, depending on the individual. Despite the limited fossil record for the 11th rib, the adult individuals K2, but especially Regourdou 1 (R1) show PC2 values above those of the RdM immature individual. These higher PC2 values are related to a relatively smaller rib shaft in cranio-caudal direction and slightly more curved ribs.

We have also compared the curvature in ribs 10 and 11 of RdM and other adult Neandertals using traditional morphometrics using the head/tubercle-ventral arc (HVA/TVA) vs. head/tubercle-ventral chord (HVC/TVC) (Supplementary Material Fig. S6). Adult individuals show larger degrees of curvature. Roc de Marsal follows the modern human comparative sample pattern of curvature. In the case of adult Neandertals, Kebara 2 (K2) shows a similar trend than modern humans though it is larger, and it is found outside the variation of a relatively large male sample (n = 24). In the case of rib 11, Neandertals are above the mean (Regourdou 1; R1) or at the upper limits of the variation (K2) of our male Euroamerican comparative sample. Despite differences in curvature, both specimens are within the ranges of variation of modern humans, though K2 would be at its limits.

Discussion and conclusions

The study of Neandertal vertebrae and especially ribs have traditionally been relegated to minor chapters, mainly inventories in longer monographs where other anatomical regions (especially the skull, the dentition and the long bones) were studied more indepth (e.g., Boule 1911-13; Heim 1976). In more recent years, the systematic re-assessment of Neandertal and other *Homo* individuals has resulted in the amendment of the anatomical determination of vertebrae and ribs in many individuals such as Shanidar 3 (Franciscus and Churchill 2002), Kebara 2 (Gómez-Olivencia et al. 2009, 2018), or La Chapelle-aux-Saints 1 (Gómez-Olivencia 2013, 2015). More recently, the study of 3D virtual reconstructions of the Neandertal immature thorax indicated that the comparatively antero-posteriorly deep and cranio-caudally short ribcage of Neandertals was already present at birth (García-Martínez et al. 2020). García-Martínez et al. (2020) studied the thorax of the Mezmaiskaya 1, Le Moustier 2, Dederiyeh, and RdM individuals. The 3D reconstruction of the thorax of RdM was possible to the previous amendment of the anatomical position of both several vertebrae and ribs of this individual. In this study we have presented the anatomical criteria followed to propose this amendment and provide a detailed analytical study of selected RdM vertebrae and ribs, that complement the synthetic approach followed by García-Martínez et al. (2020).

Assigning anatomical elements as accurately as possible is a necessary step for properly assessing the Neandertal morphology in these traditionally under-studied regions. Despite the fact that the skeleton from Roc de Marsal was in articulation and was excavated within a block and then extracted in the laboratory by a technician under the direction of Prof. Jean Piveteau, it was studied and published many years later by Madre-Dupouy (1992).

In a photograph provided by Sandgathe et al. (2011) of the RdM skeleton *in situ*, we observe a minimum of 10 ribs from the left side (ribs 3-12). In her inventory, Madre-Dupouy (1992) suggests the presence of nine ribs (eight according to us) and provides a photograph (her Figure number 78; Supplementary Material Fig. S7) of the cleaning process of the thorax, in which some of the ribs and vertebrae had been already removed, and which also shows some of the ribs in poor state of preservation. In this image, six or seven ribs from the right side and ribs 7-12 from the left side are clearly visible. In this photograph, from the left side, it is possible to clearly identify #36 (8L), #28 (10L), #40 (11L), and #44 (12L) (Supplementary Material Fig. S3). From the right side, it is possible to recognize #33.2 (4R), the #302 rib cluster and #35 (7R). We have been able to identify additional postcranial remains belonging to the RdM infant among the indeterminate remains that derive from the cleaning the block that contained this individual (Gómez-Olivencia and García-Martínez 2019) and directly observed how, in some cases, the sediment adheres firmly to the human remains. We further observed some breakage, probably due to sediment compaction and the presence of small stones mixed with the sediment (Gómez-Olivencia, personal observation). Based on these observations and on our new assignments we suggest that: 1) part of the skeleton may have been destroyed during the cleaning process due to the inherent fragility of these bones; and 2) the time gap between the discovery-cleaning and the first systematic study published in 1992 could have led to the loss of important anatomical and spatial information (Supplementary Material Fig. S7). Unfortunately, to our knowledge, there is no documentation of the restoration process, which currently precludes further assessment.

Costal morphology of the Roc de Marsal infant

Madre-Dupouy (1992) emphasized three aspects of rib morphology present in RdM: their gracility, their short necks, and their large radius of curvature and a pronounced anterior flare. She interpreted these features as resulting in a thorax well-developed antero-posteriorly, with a maximum width at the 7th rib. In light of analysis of the anatomical position of the ribs of RdM, it is necessary to reassess these features. With regard to rib robusticity, Madre-Dupouy's interpretation is at odds with the assessment made by Kondo and Dodo (2003) of the subadult Neandertal Dederiyeh 1 (D1) ribs, characterized as relatively robust, with large and triangular cross sections, wide and shallow costal grooves, and similar in curvature to *H. sapiens* infants or even more strongly curved in the lower rib. Kondo and Dodo (2003) based their conclusions on two aspects of rib morphology: 1) comparison of the D1 index of rib thickness to rib height measured at the posterior angle to a sample (n = 9) of modern human infants/children ranging in age from 1 year and 2 months to about 4 years, and 2) comparison of the external morphology of the cross-sections of the left ribs of D1 to modern humans aged about 4 to 5 years (i.e., older than D1). In the latter case, the section was made at an indeterminate distance ("slight") from the posterior angle and showed a more robust aspect in D1 which would be consistent with the morphology present in adult individuals (García-Martínez et al. 2018b and references therein). The RdM robusticity index at the posterior angle shows is similar to a small modern human sample and greater than that observed for D1 in all the preserved ribs, except ribs 9 and 11 (Tab. 4). Therefore, D1 does not seem to be so robust when compared to this modern human sample (Kondo and Dodo 2003). The cross-sections of the left ribs were made at an indeterminate ("slight") distance from the posterior angle and showed a more

robust aspect in D1 which would be consistent with the morphology present in adult individuals (García-Martínez et al. 2018b and references therein). Differences in external thickness are but one aspect of bone robusticity. Future assessment of the cross-sectional distribution of cortical and trabecular bones in immature Neandertal ribs will clarify whether the pattern of thicker cortical bones found in long bones (Kondo and Dodo 2003) are also present in ribs.

Madre-Dupouy's (1992) assessment of the RdM neck length is based on what she believed to be the fourth rib. Our reassessment of this specimen suggests that this is a 10th rib, and thus neck morphology corresponds more to what would be expected from a rib from the lower thorax, i.e., shorter in comparison to ribs from the upper thorax ribs that display longer necks. However, as previously noted (Franciscus and Churchill 2002; García-Martínez et al. 2017), the fossil record for vertebral ends of ribs (e.g., head, neck and tubercle) for adult Neandertals is extremely limited and this is true as well for nonadult Neandertals.

Madre-Dupouy (1992) compared the outlines of ribs 4–7 from RdM to modern humans to analyze the curvature of the ribs. Our anatomical reassessment suggests that the rib identified by Madre-Dupouy (1992) as the 4th is actually a 10th rib. The visual comparison and the geometric morphometric assessment of ribs 9, 10 and 11 suggests a lower degree of curvature in RdM compared to modern humans (Figs. 3–4).

Finally, although several ribs from the Roc de Marsal assemblage are fragmentary or affected by preservation-related damage, the morphometric analyses were intentionally based exclusively on ribs 9, 10 and 11, which are preserved in their entirety and show no taphonomic alteration of their overall geometry. This conservative selection minimizes the potential influence of breakage, deformation, or reconstruction uncertainty on the results. Consequently, the detected differences in rib curvature and orientation relative to modern humans are unlikely to represent artifacts of preservation but instead reflect genuine anatomical features of the RdM thorax.

In summary, our assessment shows differences in the ribs of the RdM infant when compared to modern human children: the most complete ribs of RdM are less curved, have more vertically oriented shafts, and are straighter in external view (i.e., less sinuous). In addition, we describe for the first time the presence in ribs 9-11 of longer shafts sternal to the posterior angle in the lowermost ribs. The assessment of these features is needed in other immature Neandertals in order to determine whether the pattern we observe in RdM is representative of Neandertals. We hypothesize that these features could be related functionally and morphologically integrated to the pelvis complex. Torres-Tamayo et al. (2018) demonstrated a complex torso integration model in *Homo sapiens* in which the highest strength of covariation was found between the lowest rib levels and the ilia. In fact, differences in the pelvic morphology have also been described in immature Neandertals when compared to modern humans (Heim 1982; Kondo and Dodo 2003).

Ontogenetic implications

Our study of the RdM infant suggests the presence of anatomical features that are consistent with those present in adult Neandertals, including the presence of straighter (less sinuous) ribs, as observed on external view (Bastir et al. 2017; Gómez-Olivencia et al. 2018). This would indicate that certain differences found in the adult Neandertal ribs are already present in infancy.

Our assessment of the 11th rib, showing less curvature, seems to be at odds with the study by García-Martínez et al. (2017) suggest that Neandertals show more curved 11th ribs than modern humans, which would implicate ontogenetic changes at this level. We consider that the results obtained by García-Martínez et al. (2017) and our PCA analysis are equivalent as the same landmark protocol was used. In both cases, Neandertals are outside the range of variation of modern humans of the same age group. Moreover, when one regards with more detail García-Martínez et al.'s (2017) Figure 8b it is possible to observe how in modern humans the posterior angle is located in a more central

position in the shaft, and that this shaft is more diagonally oriented while in Neandertals the shaft is more vertically oriented (Supplementary Material Fig. S8). In our opinion, the orientation of the shaft and the position of the posterior angle affects the curvature.

In summary, our results suggest that for some ribs, the pattern of curvature and shaft orientation detected in Neandertal adults is already present in the RdM infant. These features can thus be added to a long list of Neandertal postcranial features already present early in ontogeny (e.g., Heim 1982; García-González et al. 2009, 2024; García-Martínez et al. 2020). Caution is warranted, however, due to the limited number of complete Neandertal remains available, as well as the subtlety of the morphological differences. It is important to conduct additional studies on modern humans assessing other aspects, such as static allometry, in order to quantify how many of the perceived differences between Neandertals and modern human are related to differences in size.

Summary and conclusions

Here we have presented a study of isolated vertebrae and ribs of the RdM Neandertal infant in which we have combined traditional and geometric morphometrics. These methodologies complement each other and provide complementary results and a better assessment of differences in the form (i.e., size plus shape) of the studied elements (see also Arlegi et al. 2017). RdM provides, additionally, a rare opportunity to study the interrelationship between the spine and the costal skeleton, and the previous 3D reconstruction of the thorax of RdM demonstrated significant differences in the thorax anatomy as a whole, which is consistent with the results obtained in the study of the individual elements in the present study. The RdM thorax can be characterized by a relatively and absolutely shorter thoracic spine (García-Martínez et al. 2020). Despite its short thoracic spine, it is very likely that the ribcage of RdM was larger (volumetrically) because its thorax was antero-posteriorly deeper (which confirms Madre-Dupouy's suggestion) and slightly wider than in modern human infants (García-Martínez et al. 2020). This fact reinforces the idea that the information found in the individual elements, the ribs and vertebrae, provides information regarding the entire thorax distinctiveness. The study of additional isolated vertebral and costal remains will, without doubt, provide a better understanding into the Neandertal thoracic variation in the future.

Author contribution

All authors contributed to the conception of the work. They also were involved in drafting or revising the article critically for intellectual content. All approved the final version.

Acknowledgements

We would like to thank C. Cretin, J.-J. Cleyet-Merle, P. Jaquement, S. Madeleine (Musée National de Prehistoire) for the permission, access and technical support during our stay in Les Eyzies. Thanks also to Yoel Rak, Israel Hershkovitz (Tel Aviv University), Yohannes Haile-Selassie (Cleveland Museum of Natural History) for access to the important collections under their care. We would like to acknowledge Dr. Wolfgang Recheis for providing access to the Innsbruck Hospital CT data. We would like to further thank the research groups from PACEA, University of the Basque Country and the Paleoanthropology group from the MNCN-Madrid and K. Willetts for fruitful discussions. Lauren Ames kindly reviewed the English of a previous version of this article. This work was supported by Research Groups IT1418-19 and IT1485-22 (Eusko Jaurlaritza-Gobierno Vasco), and by Spanish Ministerio de Ciencia e Innovación (Projects PGC2018-093925-B-C33, MCI/AEI/FEDER, UE, PID2021-122355NB-C31, MCIN/AEI/10.13039/501100011033/FEDER, UE) and by Spanish Ministerio de Ciencia, Innovación y Universidades (Project PID2024-156477NB-C33 financed by MICIU/AEI/10.13039/501100011033/FEDER, UE) and Ministerio de Economía y Competitividad (CGL2015-63648P). DGM was funded by the

"Juan de la Cierva Formación" program (FJCI-2017-32157) from the Spanish Ministerio de Ciencia, Innovación y Universidades, by the IdEx University of Bordeaux Investments for the Future program (ANR-10-IDEX-03-02). We would like to thank the reviewers, the associate editor and the editor that provided very useful comments in previous versions of this paper.

References

Arlegi M, Gómez-Olivencia A, Albessard L, et al (2017) The role of allometry and posture in the evolution of the hominin subaxial cervical spine. J Hum Evol 104:80-99. http://dx.doi.org/10.1016/j.jhevol.2017.01.002

Arsuaga JL, Carretero JM, Lorenzo C, et al (2015) Postcranial morphology of the middle Pleistocene humans from Sima de los Huesos, Spain. Proc Natl Acad Sci U S A 112:11524–11529. http://doi.org/10.1073/pnas.1514828112

Arsuaga JL, Lorenzo C, Carretero JM, et al (1999) A complete human pelvis from the Middle Pleistocene of Spain. Nature 399:255–258. https://doi.org/10.1038/20430

Bastir M, García Martínez D, Rios L, et al (2017) Three-dimensional morphometrics of thoracic vertebrae in Neandertals and the fossil evidence from El Sidrón (Asturias, Northern Spain). J Hum Evol 108:47–61. https://doi.org/10.1016/j.jhevol.2017.03.008

Bastir M, García-Martínez D, Estalrrich A, et al (2015) The relevance of the first ribs of the El Sidrón site (Asturias, Spain) for the understanding of the Neandertal thorax. J Hum Evol 80:64–73. http://dx.doi.org/10.1016/j.jhevol.2014.10.008

Bastir M, García-Martínez D, Torres-Tamayo N, et al (2020) Rib cage anatomy in *Homo erectus* suggests a recent evolutionary origin of modern human body shape. Nat Ecol Evol 4:1178–1187. https://doi.org/10.1038/s41559-020-1240-4

Bastir M, García-Martínez D, Torres-Tamayo N, et al (2019) Workflows in a Virtual Morphology Lab: 3D scanning, measuring, and printing. J Anthropol Sci 97:107–134. https://doi.org/10.4436/jass.97003

Bayle P, Braga J, Mazurier A, et al (2009) Dental developmental pattern of the Neanderthal child from Roc de Marsal: a high-resolution 3D analysis. J Hum Evol 56:66–75. http://dx.doi.org/10.1016/j.jhevol.2008.09.002

Been E, Gómez-Olivencia A, Kramer PA, et al (2017) 3D reconstruction of spinal posture of the Kebara 2 Neandertal. In: Marom A, Hovers E (eds) Human paleontology and prehistory: Contributions in honor of Yoel Rak, Springer, p. 239–251. https://doi.org/10.1007/978-3-319-46646-0_18

Bonmatí A, Gómez-Olivencia A, Arsuaga JL, et al (2010) Middle Pleistocene lower back and pelvis from an aged human individual from the Sima de los Huesos site, Spain. Proc Natl Acad Sci U S A 107:18386–18391. https://doi.org/10.1073/pnas.1012131107

Bookstein FL (1991) Morphometric tools for landmark data: geometry and biology, Cambridge University Press, Cambridge.

Boule M (1911–1913) L'homme fossile de la Chapelle aux Saints. Annales de Paléontologie 6:111–172; 7:21–56, 85–192; 8:1–70.

Bordes F, Lafille J (1962) Découverte d'un squelette d'enfant moustérien dans le gisement du Roc de Marsal, commune de Campagne-du-Bugue (Dordogne). C R Acad Sci 254:714–715.

Carretero JM, Arsuaga JL, Martínez I, et al (2004) Los humanos de la Sima de los Huesos (Sierra de Atapuerca) y la evolución del cuerpo en el género *Homo*. In: Baquedano E, Rubio S (eds) Miscelánea en homenaje a Emiliano Aguirre. Volumen III. Paleoantropología, Museo Arqueológico Regional, Alcalá de Henares, p. 120–135.

Cirillo J, Henneberg M (2012) Sequencing human ribs into anatomical order by quantitative multivariate methods. Homo 63:182–201. https://doi.org/10.1016/j.jchb.2012.04.001

Dudar JC (1993) Identification of rib number and assessment of intercostal variation at the sternal rib end. J Forensic Sci 38:788–797. https://doi.org/10.1520/JFS13474J

Duday H, Arensburg B (1991) La pathologie. In: Bar-Yosef O, Vandermeersch B (eds) Le squelette moustérien de Kébara 2, Éditions du CNRS, Paris, p. 180–193.

Fedorov A, Beichel R, Kalpathy-Cramer J, et al (2012) 3D Slicer as an image computing platform for the Quantitative Imaging Network. Magn Reson Imaging 30:1323–1341. https://doi.org/10.1016/j.mri.2012.05.001

Franciscus RG, Churchill SE (2002) The costal skeleton of Shanidar 3 and a reappraisal of Neandertal thoracic morphology. J Hum Evol 42:303–356. https://doi.org/10.1006/jhev.2001.0528

García-González R, Carretero JM, Rodríguez L, et al (2009) Étude analytique d'une clavicule complète de subadulte d'*Homo antecessor* (site de Gran Dolina, Sierra d'Atapuerca, Burgos, Espagne). L'anthropologie 113: 222–232. https://doi.org/10.1016/j.anthro.2008.12.002

García-González R, Rodríguez L, Salazar-Fernández A, et al (2024) Updated study of adult and subadult pectoral girdle bones from Sima de los Huesos site (Sierra de Atapuerca, Burgos, Spain). Anatomical and age estimation keys. Anat Rec 307:2491–2518. https://doi.org/10.1002/ar.25158

García-Martínez D, Barash A, Recheis W, et al (2014) On the chest size of Kebara 2. J Hum Evol 70:69–72. http://dx.doi.org/10.1016/j.jhevol.2014.02.003

García-Martínez D, Bastir M, Gómez-Olivencia A, et al (2020) Early development of the Neanderthal ribcage reveals a different body shape at birth compared to modern humans. Sci Adv 6:eabb4377. https://doi.org/10.1126/sciadv.abb4377

García-Martínez D, Bastir M, Huguet R, et al (2017) The costal remains of the El Sidrón Neanderthal site (Asturias, northern Spain) and their importance for understanding Neanderthal thorax morphology. J Hum Evol 111:85–101. https://doi.org/10.1016/j.jhevol.2017.06.003

García-Martínez D, Campo Martín M, González Martín A, et al (2018a) Reevaluation of 'endocostal ossifications' on the Kebara 2 Neanderthal ribs. J Hum Evol 122:33–37. https://doi.org/10.1016/j.jhevol.2018.04.011

García-Martínez D, Radovčić D, Radovčić J, et al (2018b) Over 100 years of Krapina: New insights into the Neanderthal thorax from the study of rib cross-sectional morphology. J Hum Evol 122:124–132. https://doi.org/10.1016/j.jhevol.2018.05.009

García-Martínez D, Torres-Tamayo N, Torres-Sanchez I, et al (2016) Morphological and functional implications of sexual dimorphism in the human skeletal thorax. Am J Phys Anthropol 161:467–477. https://doi.org/10.1002/ajpa.23051

García-Martínez D, Torres-Tamayo N, Torres-Sanchez I, et al (2018c). Ribcage measurements indicate greater lung capacity in Neanderthals and Lower Pleistocene hominins compared to modern humans. Commun Biol 1:117. https://doi.org/10.1038/s42003-018-0125-4

Gómez-Olivencia A (2013) Back to the old man's back: Reassessment of the anatomical determination of the vertebrae of the Neandertal individual of La Chapelle-aux-Saints. Ann Paléontolog 99:43–65. http://dx.doi.org/10.1016/j.annpal.2012.07.002

Gómez-Olivencia A (2015) The costal skeleton of the Neandertal individual of La Chapelle-aux-Saints 1. Ann Paléontolog 101:127–141. http://dx.doi.org/10.1016/j.annpal.2015.04.005

Gómez-Olivencia A, Barash A, García-Martínez D (2018) 3D virtual reconstruction of the Kebara 2 Neandertal thorax. Nat Commun 9:4387. https://doi.org/10.1038/s41467-018-06803-z

Gómez-Olivencia A, Carretero JM, Lorenzo C, et al (2010) The costal skeleton of *Homo antecessor*: preliminary results. J Hum Evol 59:620–640. https://doi.org/10.1016/j.jhevol.2010.07.023

Gómez-Olivencia A, Couture-Veschambre C, Madelaine S, et al (2013) The vertebral column of the Regourdou 1 Neandertal. J Hum Evol 64:582–607. http://dx.doi.org/10.1016/j.jhevol.2013.02.006

Gómez-Olivencia A, Eaves-Johnson KL, Franciscus RG, et al (2009) Kebara 2: new insights regarding the most complete Neandertal thorax. J Hum Evol 57:75–90. https://doi.org/10.1016/j.jhevol.2009.02.009

Gómez-Olivencia A, García-Martínez D (2019) New postcranial remains from the Roc de Marsal Neandertal child. Paleo 30:164–169. https://doi.org/10.4000/paleo.4631

Gómez-Olivencia A, Holliday T, Madelaine S, et al (2019) The costal skeleton of the Regourdou 1 Neandertal. J Hum Evol 130:151–171. https://doi.org/10.1016/j.jhevol.2017.12.005

Goodyear MDE, Krleza-Jeric K, Lemmens T, (2007) The declaration of Helsinki. BMJ 335:624–625. https://doi.org/10.1136/bmj.39339.610000.BE

Gunz P, Mitteroecker P, Bookstein FL (2005) Semilandmarks in three dimensions. In: Slice D (ed) Modern morphometrics in physical anthropology. Kluwer Academic/Plenum Publishers, New York, p. 73–98.

Heim J-L (1982) Les enfants néandertaliens de la Ferrassie. Étude anthropologique et analyse ontogénique des hommes de Néandertal, Masson, Paris.

Holliday TW (2012) Body size, body shape, and the circumscription of the genus *Homo*. Current Anthropol 53, S330–S345. https://doi.org/10.1086/667360

Kondo O, Dodo Y (2003) The postcranial bones of the Neanderthal child of burial nº1. In: Akazawa T, Muhesen T (eds) Neanderthal burials. Excavations of the Dederiyeh Cave, Afrin, Syria, KW Publications Ltd., Auckland, p. 93–137.

Lafille J (1961) Le gisement dit «Roc de Marsal», commune de Campagne du Bugue (Dordogne): note préliminaire. Bull Soc Préhistorique Française 58:712–713.

Madre-Dupouy M (1992) L'enfant du Roc de Marsal. Éditions du CNRS, Paris.

Mann RW (1993) A Method for siding and sequencing human ribs. J Forensic Sci 38:151–155. https://doi.org/10.1520/JFS13388J

Rak Y (1991) The pelvis. In: Bar-Yosef O, Vandermeersch B (eds), Le squelette moustérien de Kébara 2. Éditions du CNRS, Paris, pp. 148–156.

Rosenberg KR, Züne L, Ruff CB (2006) Body size, body proportions, and encephalization in a Middle Pleistocene archaic human from northern China. Proc Natl Acad Sci USA 103:3552–3556. https://doi.org/10.1073/pnas.0508681103

Sandgathe DM, Dibble HL, Goldberg P, et al (2011) The Roc de Marsal Neandertal child: A reassessment of its status as a deliberate burial. J Hum Evol 61:243–253. https://doi.org/10.1016/j.jhevol.2011.04.003

Trinkaus E (2011) The postcranial dimensions of the La Chapelle-aux-saints 1 Neandertal. Am J Phys Anthropol 145:461–468. https://doi.org/10.1002/ajpa.21528

Turq A (1989) Le squelette de l'enfant du Roc de Marsal. Les données de la fouille. Paleo 1:47–54. https://doi.org/10.3406/pal.1989.952

Weinstein KJ (2008) Thoracic morphology in Near Eastern Neandertals and early modern humans compared with recent modern humans from high and low altitudes. J Hum Evol. 54:287–295. https://doi.org/10.1016/j.jhevol.2007.08.010

Williams SA (2012) Placement of the diaphragmatic vertebra in catarrhines: Implications for the evolution of dorsostability in hominoids and bipedalism in hominins. Am J Phys Anthropol 148:111–122. https://doi.org/10.1002/ajpa.22049

Williams SA, Middleton ER, Villamil CI, et al (2016) Vertebral numbers and human evolution. Am J Phys Anthropol 159:19–36. https://doi.org/10.1002/ajpa.22901

Zelditch M, Swiderski D, Sheets H (2012) Geometric morphometrics for biologists. 2nd Edition. Academic Press, New York.

Associate Editor, Fabio De Vincenzo